



Delivery of Allogeneic Adipose Stem Cells in Polyethylene Glycol-Fibrin Hydrogels as an Adjunct to Meshed Autografts After Sharp Debridement of Deep Partial Thickness Burns

DAVID M. BURMEISTER , RANDOLPH STONE II, NICOLE WRICE, ALFRED LABORDE, SANDRA C. BECERRA, SHANMUGASUNDARAM NATESAN, ROBERT J. CHRISTY

Key Words. Burns • Skin • Grafts • Stem cells • Hydrogels • Tissue engineering

^aBurn Injury Research, United States Army Institute of Surgical Research, JBSA Fort Sam Houston, Texas, USA

Correspondence: Robert J. Christy, Ph.D., Burn Injury Research, United States Army Institute of Surgical Research, 3698 Chambers Pass, BHT1: Building 3611, JBSA Fort Sam Houston, Texas 78234-6315, USA. Telephone: 210-539-9528; e-mail: robert.j.christy12.civ@mail.mil

Received June 19, 2017; accepted for publication December 11, 2017; first published February 18, 2018.

<http://dx.doi.org/10.1002/sctm.17-0160>

This is an open access article under the terms of the Creative Commons Attribution-NonCommercial-NoDerivs License, which permits use and distribution in any medium, provided the original work is properly cited, the use is non-commercial and no modifications or adaptations are made.

ABSTRACT

Harvesting of autografts results in donor site morbidities and is limited in scenarios such as large total body surface area burns. In these instances, coverage is increased by meshing grafts at the expense of delayed biologic closure. Moreover, graft meshing increases the likelihood of contraction and hypertrophic scarring, limits range of motion, and worsens cosmesis. Many tissue engineering technologies have touted the promise of adipose-derived stem cells (ASCs) for burn wounds. The primary objective of the current study was to determine feasibility and efficacy of in situ ASC delivery via PEGylated fibrin (FPEG) hydrogels as adjuncts to meshed split thickness skin grafts in a porcine model. Deep partial thickness burns were created on the dorsum of anesthetized Yorkshire pigs, and subsequently debrided on post-burn day 4. After debridement, wounds were treated with: split thickness skin grafts (STSG); meshed STSG (mSTSG); and mSTSG + FPEG with increasing doses of ASCs. We show that FPEG hydrogels can be delivered in situ to prevent the contraction seen after meshing of STSG. Moreover, ASCs delivered in FPEG dose-dependently increase blood vessel size which significantly correlates with CD31 protein levels. The current study reports a dual-action adjunct therapy to autografting administered in situ, wherein FPEG acts as both scaffolding to prevent contraction, and as a delivery vehicle for ASCs to accelerate angiogenesis. This strategy may be used to incorporate other biologics for generating tissue engineered products aimed at improving wound healing and minimizing donor sites or scarring. *STEM CELLS TRANSLATIONAL MEDICINE* 2018;7:360–372

SIGNIFICANCE STATEMENT

Patients with second- and third-degree burn wounds undergo surgical removal of necrotic tissue and grafting with skin taken from elsewhere on their body. Harvesting donor skin is painful and creates another wound on the patient. This study uses a preclinical porcine burn model to show that donor sites can be minimized by delivering subcutaneous fat-stem cells in polyethylene-glycol-fibrin-based hydrogels. This combination works by preventing contraction and increasing blood vessel size in the burn wound for improved healing. This approach can theoretically be performed using the patients' own isolated stem cells and plasma, thus improving outcomes in immunocompromised burned victims.

INTRODUCTION

The incidence of burns requiring medical attention worldwide is near 11 million people, making burns the fourth most common injury on the planet [1]. Full and deep partial thickness burns have complete destruction of the epidermis, resulting in a lack of hair follicle stem cells for re-epithelialization and skin regeneration. For decades, the treatment strategy for deep burn wounds has been excision of necrotic tissue and grafting for coverage of the exposed wound bed [2] which

has been shown to decrease the rate of infection, hospital stays, and mortality [3]. The gold standard for coverage is a split-thickness skin graft (STSG) from a donor site elsewhere on the patient (i.e., autograft). While these autografts have inherent biocompatibility, harvesting them is associated with various comorbidities including prolonged immobility and donor site pain [4, 5]. Moreover, autograft availability is often not feasible with extensive burn wounds covering a large percentage of total body surface area [6].

In these scenarios, it has become common practice to mesh skin grafts at various ratios, either manually or mechanically [7]. Skin meshing increases the wound surface area covered (thus minimizing donor sites) and has also been shown to reduce the incidence of hematoma formation [8, 9]. Despite these advantages, concerns over ultimate cosmesis and healing rates exist, because of the increased contraction compared with unmeshed/unexpanded grafts [10]. The face, neck, and hands are especially problematic because of contraction-related impairments in range of motion [11]. To combat these problems, many investigations into tissue-engineered skin equivalents have recently occurred [12, 13]. While a number of products incorporate autologous keratinocytes for epidermal replacement, the ensuing graft is only several cell layers thick, and thus prone to breakdown/infection [14]. Moreover, these technologies require several weeks for culturing autologous cells after biopsy. Dermal replacements without cells (e.g., Integra, Alloderm) are usually used in a two-step process due to the time required for incorporation with host tissue prior to definitive grafting. In short, no available treatment has proven as effective as autografts for reasons such as rejection and insufficient vascularization [15–17].

To this end, several populations of stem cells have been investigated for their therapeutic benefit in burn wound healing [18, 19]. Adipose-derived stem cells (ASCs) are a type of mesenchymal stem cell that possess immunosuppressive activity [20–22], making their allogeneic use possible. ASCs also show strong angiogenic activity via paracrine mechanisms [23]. ASCs are easy to isolate from lipos aspirate with sufficient yield [24], including from excised tissue from burn patients [25]. Taken together, these properties make ASCs an attractive candidate for enhancing burn wound healing. However, conflicting evidence exists on the efficacy of ASCs on burns [26, 27], possible owing to delivery strategies. One delivery method involves modification of fibrin by crosslinking with polyethylene glycol (FPEG) to deliver ASCs. This strategy has recently been shown to enhance vascularization in excisional wounds in nude rats [28, 29]. The chemical alteration (i.e., PEGylation) of fibrin also increases stability and decreases degradation rates of thrombin-mediated hydrogels [30, 31], while maintaining angiogenic and antimicrobial activity [32]. Although augmenting the natural angiogenic activity of fibrin with delivery of ASCs has great potential for therapy in burns, this has currently not been explored in detail.

To this end, the current study uses a porcine model of deep partial thickness burns with subsequent excision and grafting. Pigs are widely regarded as the best preclinical surrogate for human skin due to their similarities in both structure and wound healing [33, 34]. Not only do pigs have similar epidermal:dermal ratios to human skin, but they also heal mainly by reepithelialization as opposed to contraction, illustrating their superiority as a translational preclinical model. Herein, we show successful isolation of subcutaneous porcine ASCs (pASCs) and demonstrate their ability to expand within FPEG hydrogels formed in situ. We then use this combination as an adjunct therapy with meshed autografts for debrided burn wounds. We show that FPEG hydrogels decrease contraction seen after graft meshing, and can also deliver ASCs which increases blood vessel size seen within the graft and surrounding granulation tissue.

MATERIALS AND METHODS

Isolation and Characterization of Porcine ASCs

All chemicals were purchased from Sigma-Aldrich (St. Louis, MO) unless otherwise specified. Subcutaneous fat was isolated from

the nape of anesthetized Yorkshire pigs (Midwest Research Swine, Gibbon, MN), finely minced with scissors, resuspended in Hank's balanced salt solution (HBSS), and centrifuged for 10 minutes at 500g at 16°C. For every 2 ml of floating tissue, 10 mg of collagenase type II (Thermo Fisher Scientific, Waltham, MA) was added and the mixture was shaken at 125 rpm for 60–90 minutes at 37°C. Undigested tissue was removed by sequential passage through 100- and 70- μ m nylon filters, and the filtrate was then washed twice with HBSS. The final cell pellets were resuspended in growth media (Mesen-PRO RS, Life Technologies, Carlsbad, CA) containing antibiotics/glutamine (100 U/ml of penicillin G, 100 μ g/ml streptomycin sulfate, 0.25 μ g/ml amphotericin B, and 2 mM of L-glutamine [Thermo]).

Three isolates of pASCs were analyzed for their differentiation capacity as previously described [35]. Adipogenic induction media consisted of high glucose (4.5 g/l) Dulbecco's modified Eagle's media (DMEM) supplemented with 10% fetal bovine serum (FBS), antibiotics/glutamine, 1 μ M dexamethasone, 200 μ M indomethacin, 10 μ M insulin, 0.5 μ M isobutylmethylxanthine, and 10 μ M ciglitazone. Adipogenesis was identified by Oil Red O staining. Osteogenic induction media consisted α MEM supplemented with 10% FBS, antibiotics/glutamine, 0.1 μ M dexamethasone, 50 μ M ascorbate-2-phosphate, 10 mM β -glycerophosphate, and 10 ng/ml bone morphogenic protein-2 (R&D Systems, Minneapolis, MN). Osteogenesis was assessed by alizarin red S staining.

RNA Extraction and Reverse Transcription Polymerase Chain Reaction (RT-PCR)

Gene expression was analyzed for stem cell, adipogenic, and osteogenic markers. RNA was isolated using Trizol LS (Thermo) incubated for 10–15 minutes on ice, followed by addition of chloroform and centrifugation. RNA was isopropanol-precipitated, purified using the RNeasy Mini kit (Qiagen, Valencia, CA), and cDNA subsequently synthesized. Porcine-specific primers (Qiagen) were used to evaluate expression of markers for mesenchymal stem cells: CD73, CD90, CD105, and CD45; adipogenesis: CEBPA (CCAAT/enhancer binding protein- α), PPARG (peroxisome proliferator activated receptor- γ), LPL (lipoprotein lipase), and ADIPOQ (adiponectin); and osteogenesis: RUNX2 (runt related transcription factor 2), IBSP (integrin-binding sialoprotein), ALPL (alkaline phosphatase), and BMP2 (bone morphogenic protein-2). Master mixes with 200 nM of primers, SYBR Select Master Mix (Thermo), and cDNA were analyzed using a Bio-Rad CFX96 (Bio-Rad, Hercules, CA). Non-template control and no reverse transcriptase controls were run for each reaction. Gene expression was normalized to ACTG1, B2M, and GAPDH, and the fold change in expression was determined by the $2^{-\Delta\Delta C_T}$ method. pASCs were compared with a previously characterized line of bone marrow stem cells (BMSCs) for stem cell/differentiation marker expression [36].

Stem Cell Marker Immunofluorescence

Immunofluorescence was performed to detect presence of stem cell markers. pASCs on chamber slides were fixed with 4% paraformaldehyde (PFA) for 20 minutes, blocked for 1 hour in 2% bovine serum albumin (BSA)/HBSS, and stained with antibodies for CD73-FITC (BD Biosciences, San Jose, CA), CD90-APC (Abcam, Cambridge, MA), CD105-PE (Abcam), and a negative control CD45-FITC (Bio-Rad).

FPEG Hydrogels

FPEG hydrogels containing pASCs were prepared as previously described [28]. Succinimidyl glutarate modified PEG (SG-PEG-SG, 3,400 Da; NOF America Corporation, White Plains, NY) was added to fibrinogen in a 1:10 molar concentration ratio in tris-buffered saline, pH 7.8, and incubated for 20 minutes at 37°C. Isolated pASCs (50,000, 250,000, and 500,000 pASCs/ml of hydrogel mixture) were added to PEG-fibrinogen. To initiate gelation, an equal volume of thrombin in 40 mM of CaCl₂ (12.5 U/ml final concentration) was added 10 minutes at 37°C. Growth media was added and changed every 2–3 days. Digital images were taken over time and media collected on days 1, 7, and 14 for detecting vascular endothelial growth factor (VEGF-A), Angiopoietin-1 (Ang-1), and basic fibroblast growth factor (b-FGF) levels via enzyme-linked immunosorbent analysis according to manufacturer's instructions (R&D Systems).

Cryopreservation and Immunofluorescence of pASCs Cultured in FPEG Hydrogels

pASC-FPEG hydrogels were cryopreserved and embedded using a gradient sucrose technique [37]. Hydrogels were washed with HBSS, fixed with 4% PFA for 20 minutes, and exposed to increasing concentrations of sucrose (5%–20%, 30 minutes each), and incubated overnight with 20% sucrose at 4°C. Samples were then embedded in a 20% Sucrose-Histoprep (Fisher Scientific, Pittsburgh, PA) mixture and frozen by liquid nitrogen-cooled isopentane. Cryosections (10 μm) were cut, washed with HBSS, and fixed with 4% PFA for 20 minutes. Samples were stained with Rhodamine Wheat Germ (1:500, Vector Labs, Burlingame, CA) for 1 hour at room temperature (RT), and mounted using Prolong Gold with DAPI (Thermo). Fluorescence images were captured using Zeiss inverted microscope (Carl Zeiss, Thornwood, NY).

Animals

Female Yorkshire swine ($N = 6$) weighing 41.0 ± 2.9 kg were used in this study. Animals had ad libitum access to food and water, and were allowed to acclimate to the facilities for at least 7 days. The animal protocol was approved by the Institutional Animal Care and Use Committee, U.S. Army Institute of Surgical Research. This study has been conducted in compliance with the Animal Welfare Act, the implementing Animal Welfare Regulations, and the principles of the Guide for the Care and Use of Laboratory Animals.

Anesthesia

Animals were fasted the night before anesthetic events. Prior to anesthesia for the burn and debridement procedures (days 0 and 4, respectively), the pig was premedicated with glycopyrrolate (0.01 mg/kg, IM) to minimize salivation and bradycardia, and a transdermal fentanyl patch (100 μg/hour) was placed on the ear. Anesthesia was induced with intramuscular-injected (IM) tiletamine-zolazepam (6 mg/kg). Animals were then intubated and placed on an automatic ventilator adjusted to maintain an end tidal PCO₂ of 40 ± 5 mmHg, maintained with 1%–3% isoflurane in 100% oxygen. In order to obtain punch biopsies and photographs, animals were sedated with IM ketamine (10–20 mg/kg) and maintained under mask anesthesia (3%–5% isoflurane).

Thermal Injury

Deep partial thickness burn wounds were created as described previously [38]. Briefly, the dorsum was shaved and sterilized with

chlorohexidine. Three-centimeter brass probes were heated to 100°C and handled with a spring-loaded insulated device for consistent pressure [39], which measured 0.9 ± 0.05 kg/cm². Heated probes were applied to the skin within tattoo markings for 25 seconds, which has previously been shown to produce deep partial thickness burns via both histological and noninvasive methods [40–42]. Twelve wounds were created on each animal, with six on either side of the spine. Wounds were then covered with a nonadherent gauze (Telfa, Tyco Healthcare, Mansfield, MA) secured in place with Elastikon surgical tape (Johnson and Johnson, New Brunswick, NJ) and finally covered with antibiotic loban (3M, St. Paul, MN).

Debridement and Treatments

On day 4 post-burn, dressings were removed for sharp debridement as described previously [38]. Tangential excision was performed until viable tissue (i.e., active bleeding) was reached, which was confirmed histologically to span from the deep dermis into the subcutaneous fat (Fig. 1A, 1B). Autografts were prepared from the animals hindlimbs using a pneumatic dermatome (Zimmer, Warsaw, IN) at 14/1,000th inch. The STSGs were constantly kept moist with sterile saline, including during meshing at a 1:1.5 ratio with a mechanical mesher (Zimmer). After debridement and graft harvesting, wounds were treated with one of the following: STSG; meshed STSG (mSTSG); mSTSG + FPEG (mSTSG + FPEG); or mSTSG + FPEG + pASCs in increasing amounts of pASCs/ml (50k, 250k, and 500k). Treatment groups were randomized beforehand and distributed equally so that every animal received a minimum of three wounds that received mSTSG + FPEG treatment. Moreover, different treatments were randomized anatomically, as variation in wound healing on the cranio-caudal axis has been shown previously [43]. Grafts were sutured along the edge of the debrided burn wound, and hydrogels (described below) were applied in situ after autografting.

FPEG hydrogels containing pASCs were prepared as described above, with modifications for in situ delivery. pASCs were added to the mixture of fibrinogen (11/mg/ml) and PEG (1.1 mg/ml) before drawing into a 10-ml syringe of a Fibrijet dual syringe applicator (Nordson, St. Paul, MN). For gelation, the 1-ml syringe was filled with a mixture of 220 μl of 40 mM CaCl₂, 165 μl of 1kU/ml thrombin, and 615 μl of diH₂O. The syringe applicator was used to mix the thrombin and FPEG together via a low viscosity tip (SA-3678, Nordson) applying a stream to deliver a 2-ml hydrogel consisting of 50k, 250k, or 500k pASCs/ml to each burn wound. Hydrogels were allowed to polymerize within the wound bed for 1 minute, which is sufficient time for full polymerization [38]. Finally, bolsters created with Xeroform (Covidien, Mansfield, MA) and saline-soaked gauze were held into place with the existing sutures, and dressed as above.

Documentation of Wound Healing and Biopsies

On post-burn days 10, 14, 21, 28, and 42, dressings were removed and digital pictures of each wound (Nikon D3000, Nikon, Melville, NY) were acquired with a four-sided ruler. Image analysis was performed with ImagePro software version 6.2 (Media Cybernetics, Bethesda, MD). For quantification of wound contraction, photographs were spatially calibrated on all four sides, and tattoos were traced with the polygon measurement tool. Eight millimeter biopsy punches were taken from the periphery of each wound bed (except day 28), with half used for histology and half snap frozen for protein analysis.

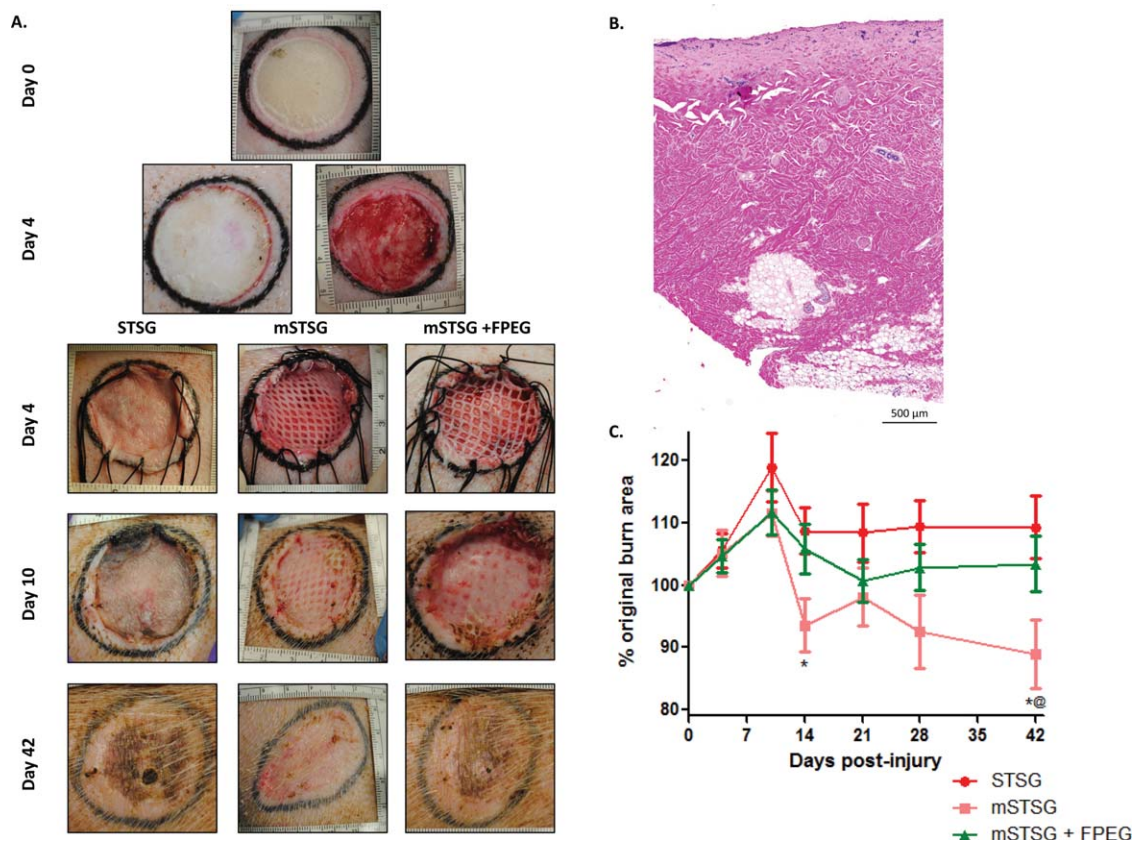


Figure 1. Photomicrographs and contraction of wounds treated with autografts. **(A):** Representative deep partial thickness burn wound (top) shows progression to day 4 post-burn, at which point wounds are debrided (2nd row right image). After debridement, wounds are covered with autografts with (mSTSG ± FPEG) and without (STSG) meshing (3rd row). Wounds on day 10 post-burn illustrate graft take, while contraction can be observed in day 42 post-burn wounds by comparing the tattoo markings. **(B):** Histological representation of debrided tissue shows excision spanned from the deep dermis into the subcutaneous adipose tissue. **(C):** Quantification shows enhanced contraction when autografts are meshed (mSTSG) compared with both nonmeshed grafts and those supplemented with FPEG. *, $p < .01$ versus STSG, *[@], $p < .05$ versus mSTSG + FPEG. Abbreviations: FPEG, PEGylated fibrin; mSTSG, meshed STSG; STSG, split thickness skin grafts.

Histopathology

Biopsies taken at each time point (minimum $n = 4$ samples/group/timepoint) were fixed in 10% buffered formalin for 48 hours, processed, embedded in paraffin, and sectioned at 6 μ m. Slides were deparaffinized in xylene, rehydrated to water, and collagen stained with Picrosirius Red (Polysciences, Warrington, PA). For analysis of blood vessels and angiogenesis, immunohistochemistry was performed with alpha smooth muscle actin (α -SMA) CD31, and VEGF-A. Heat-mediated antigen retrieval with 0.01 M citrate buffer at 95°C–98°C for 15 minutes was followed by an endogenous peroxidase block with 0.3% H₂O₂ for 20 minutes at RT. Nonspecific IgG was blocked with 10% horse serum in HBSS for 30 minutes at RT, and sections were then incubated with Abcam antibodies against α -SMA (ab7817, 1:50), CD31 (ab28364, 1:50) and VEGF-A (ab46154, 1:500) for 60 minutes at RT. Slides were washed with HBSS and treated with biotinylated anti-mouse secondary antibody (Vector Labs) for 60 minutes. Finally, immunostaining was completed with 30 minutes incubation with Vectastain-RTU Kit solution (Vector) followed by 5–10 minutes incubation with ImmPACT DAB (Diaminobenzidine, Vector) at RT. Slides were counterstained with hematoxylin and dehydrated for cover slipping.

Histopathology quantification was performed for blood vessels, epithelial thickness, and collagen content. Quantification of

blood vessels in the entire day 10 biopsies was performed with ZEN Imaging Software after whole slide scanning in an AxioScanZ1 slide scanner (Carl Zeiss, Thornwood, NY). Separate regions of interest were generated for retained autograft and granulation tissue. All blood vessels in these areas were traced to give a total number and cross-sectional area of all vessels. Trichrome images were used for determination of epithelial thickness, which was measured in triplicate in both the grafted areas and interstices. For picrosirius red-stained samples at day 42, ImageJ software version 1.51d (Bethesda, MD) was used. The entire wound bed and surrounding normal tissue were traced as two different regions of interest (Fig. 7). The entire image was split into red, green, and blue channels, and the measurement tool was used to give mean intensity within those regions of interest for each channel.

Protein Analysis

Protein extraction was performed with ice-cold RIPA buffer (Thermo) supplemented with a protease inhibitor cocktail followed by homogenization on ice and centrifugation at 14,000g for 15 minutes. Protein concentration in the supernatant was determined with Pierce bicinchoninic acid assay (Thermo). Laemmli buffer (Bio-Rad) was prepared by adding 5% 2-mercaptoethanol and used to dilute samples to 50 μ g for loading. Proteins were denatured at 95°C for 5 minutes, and separated on Mini-

PROTEAN TGX Stain-Free 4%–15% gradient gels (Bio-Rad) for 30 minutes at 300 V, and transferred to nitrocellulose membranes with Trans-Blot Turbo (Bio-Rad).

Membranes were blocked for 30 minutes in 10% nonfat dry milk (NFDM) dissolved in TBST (Tris-buffered saline + 0.1% Tween 20). A CD31 antibody (Abbiotec, San Diego, CA) or a VEGF-A antibody (Abcam, ab46153, 1:500) was diluted 1:200 in 5% NFDM/TBST and incubated overnight at 4°C with gentle rocking. Membranes were washed (TBST), incubated with horseradish peroxidase goat anti-Rabbit IgG antibody (1:3,000 in 5% NFDM/TBST) for 1 hour at RT, and then washed again. For visualization, membranes were activated and imaged using the ChemiDoc MP imaging system (Bio-Rad). As opposed to the use of loading controls, stain-free total protein was used for normalization [44–46].

Hydroxyproline Assay

On day 42 post-burn, hydroxyproline assays were performed to measure collagen according to the manufacturer's instructions (BioVision, Milpitas, CA). Briefly 100 μ l dH₂O was used for every 10 mg of tissue, and 100 μ l of homogenate was hydrolyzed using equal volumes of concentrated HCl (~12N) at 120°C for 3 hours. Samples were transferred to a 96-well plate and evaporated to dryness at 60°C. Standard (1 mg/ml) diluted to 0.1 mg/ml was used to generate the standard curve, and to spike test samples (0.4 μ g) to ensure accurate detection of hydroxyproline. Chloramine T reagent was prepared with 100 μ l added to each sample/standard and incubated at RT for 5 minutes. After incubation with p-dimethylaminobenzaldehyde (100 μ l) reagent (90 minutes, 60°C), absorbance was measured at 560 nm.

Statistical Analysis

Statistical evaluations were performed using GraphPad Prism software (GraphPad Software, San Diego, CA). For all analyses, either a one or two-way ANOVA with Bonferroni post-hoc testing was used, and *p* values less than 0.05 were considered significant. Unless otherwise stated, all results are expressed as the arithmetic mean \pm SEM.

RESULTS

Graft Meshing Increases Contraction Which Is Reversed by Addition of FPEG

We initially aimed to establish the effects of grafting on wound contraction *in vivo*. A representative burn wound with a characteristic pale appearance is shown in Figure 1A, and progresses to day 4 with a pronounced zone of hyperemia. Debridement resulted in a viable wound bed followed by grafting with autologous STSG. Successful graft meshing is also shown, with a less obvious shiny appearance of the FPEG hydrogel on top of the mSTSG. By day 10 post-burn, adequate graft take was macroscopically seen in all groups, with noticeable granulation tissue deposition in the interstitial areas. As quantified in Figure 1B, significantly more contraction occurred in the mSTSG group compared with their nonmeshed counterparts (88.89% \pm 5.57% of the original burn area vs. 109.35% \pm 5.02%, respectively). Moreover, this was ameliorated with the addition of FPEG to the wounds (103.42% \pm 4.45%). No differences were observed in tissue thickness or reepithelialization across time as determined histologically (data not shown).

Graft take on day 10 post-burn was visualized microscopically with Masson's trichrome (Fig. 2). In the STSG group, the graft is visible spanning the wound bed, with granulation tissue present underneath the autograft. In the epithelium, mature rete ridges are also seen. In contrast, the collagen within the mSTSG group appears less dense/more disorganized than that in STSG or mSTSG + FPEG groups. However, granulation tissue rapidly filled in the interstitial spaces (Fig. 2) which were largely reepithelialized, albeit with a hyperplastic epithelium lacking rete ridges. Finally, the presence of FPEG gel on day 10 post-burn is apparent as the most superficial, amorphous layer that still allows for development of a mature stratum corneum.

Subcutaneous pASCs Express Stem Cell Markers and Have Multilineage Potential

We successfully isolated pASCs from subcutaneous fat, which were easily expanded *in vitro*. These cells were positive for mesenchymal stem cell markers CD73, CD90, and CD105, while being negative for CD45 (Fig. 3A). RT-PCR revealed no differences in expression of these markers between BMSCs and pASCs, with average Cq values of 24.23 versus 24.59 (CD73), 20.82 versus 21.54 (CD90), 24.36 versus 24.2 (CD105) and 37.34 versus 35.6 (CD45). When challenged to differentiate, pASCs were shown to be adipogenic and osteogenic via Oil Red O and alizarin red staining, respectively (Fig. 3C-F). Moreover, RT-PCR showed that differentiated cells expressed much higher levels of adipogenic and osteogenic markers than undifferentiated cells, with a fold change often higher than BMSCs.

pASCs Expand Within FPEG Hydrogels and Release VEGF

We seeded pASCs within FPEG at increasing densities of 50k, 250k, and 500k pASCs/ml of hydrogel. Figure 4A shows the dose dependent increase in cell density when pASCs are allowed to expand in FPEG gels for 14 days *in vitro*. Light micrographs and wheat germ staining reveal the dose-dependent increase in cells 1 day after mixing, with pASCs able to form connections within the FPEG hydrogels. Cell growth was supported out to 14 days, with 50k pASCs/ml showing a drastic increase in cell density compared with day 1. Last, pASCs within FPEG hydrogels released VEGF in a dose- and time- dependent fashion (Fig. 4C). Specifically, while the amount of VEGF release at day 1 is nearly proportional to the amount of cells, this difference disappears as cells in the 50K pASCs/ml hydrogels proliferate and approach the capacity of FPEG. Additionally, pASCs within the hydrogels released Ang-1, with significantly higher levels present with the highest concentration at day 7, and all concentrations of pASCs at day 14. No differences were seen in the levels of b-FGF.

Delivery of pASCs from FPEG Hydrogels Does Not Affect Contraction *In Vivo*

We next aimed to demonstrate feasibility and efficacy of delivering pASCs to the wound bed within these FPEG hydrogels. When delivered to debrided burn wounds treated with mSTSG, pASCs did not prevent or augment the beneficial effects of FPEG alone on wound contraction. On day 42 post-burn, the percentage of the original wound area was 97.0% \pm 5.90%, 94.89% \pm 6.34%, and 99.11% \pm 7.13% when 1×10^5 , 5×10^5 , and 1×10^6 pASCs, respectively, were delivered to the wound in FPEG hydrogels. In terms of epithelialization, the interstices between meshed graft areas were largely epithelialized on day 10, with one of six wounds not fully reepithelialized in both FPEG and FPEG + 250K pASCs/ml

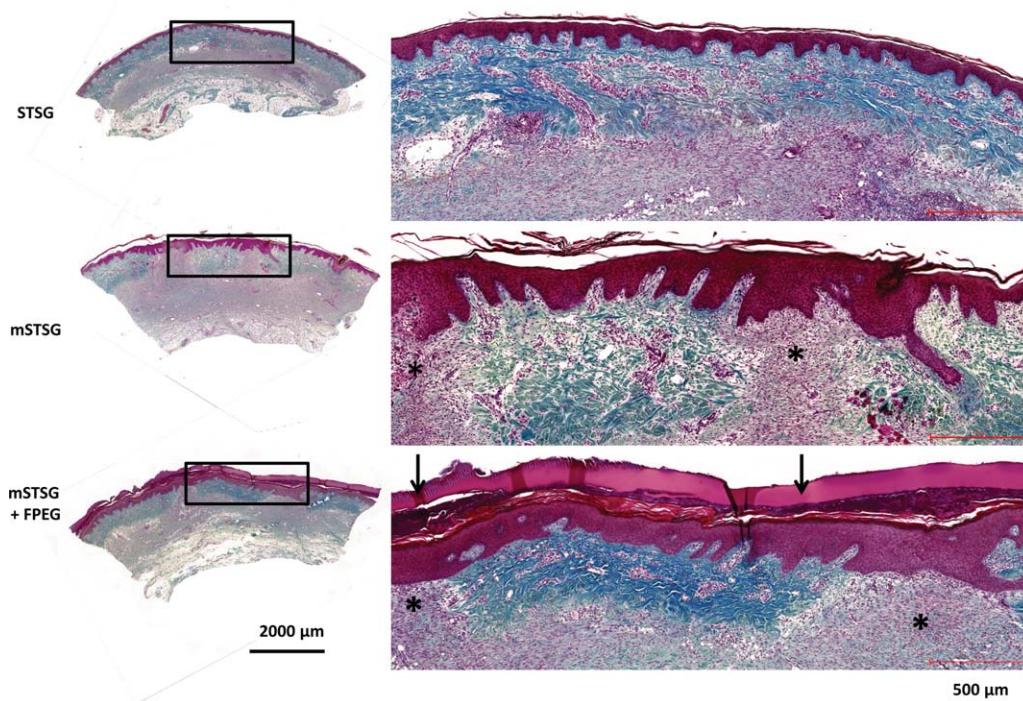


Figure 2. Microscopic appearance of grafts in wound beds on day 10 post-burn. Masson's trichrome staining on day 10 post-burn at $\times 10$ magnification. Wounds treated with intact STSG show a continuous dermal layer covering granulation tissue. The mature epithelium complete with rete ridges is also visible in the mSTSG and mSTSG + FPEG groups where the dermal layer from the graft is visible. In the interstitial spaces between autograft, significant granulation tissue (asterisks) is covered by a newly formed, hyperplastic epithelium. In the mSTSG + FPEG group, the acellular FPEG hydrogel is stained red and seen superficial to the epithelium (scale bars are 2,000 and 500 μm). Abbreviations: FPEG, PEGylated fibrin; mSTSG, meshed STSG; STSG, split thickness skin grafts.

groups. Moreover, analysis of epithelial thickness in the interstices showed a significantly hyperplastic epithelium when compared with grafted areas in all groups but the FPEG + 500 pASCs/ml group (Supporting Information Fig. 1).

Delivery of pASCs from FPEG Hydrogels Increases the Size of Blood Vessels Within Both Graft and Granulation Tissue

Representative images of immunohistochemical staining to α -SMA from day 10 post-burn biopsies are shown in Figure 5A. Measurement of the total area in day 10 biopsies revealed a trend toward increased granulation tissue deposition with pASCs. This area was $3.44 \pm 1.53 \text{ mm}^2$, $4.85 \pm 1.01 \text{ mm}^2$, $5.78 \pm 1.63 \text{ mm}^2$, and $6.25 \pm 0.45 \text{ mm}^2$ for FPEG, FPEG + 50K pASCs/ml, FPEG + 250K pASCs/ml, and FPEG + 500K pASCs/ml, respectively, which did not reach statistical significance ($p = .16$). Blood vessels were then measured in the entire biopsy and separated by graft and granulation tissue (high magnification images shown in Fig. 5B). As shown in Figure 5C, no differences were detected in the total amount of blood vessels/ mm^2 amongst groups in either the granulation tissue or the retained grafts. However, a highly significant and dose-dependent increase in the average cross-sectional area of blood vessels was seen with pASCs, which held true in both graft and granulation tissue ($p < .001$).

To examine the endothelial component of the angiogenic benefit of pASCs, immunohistochemistry and Western blotting were performed to determine the levels of CD31 (Fig. 6). Figure 6A shows representative staining for CD31 which shows a similar dose-dependent effect of pASCs at day 10 and 14, without a noticeable difference at later timepoints. Similarly to blood vessel

size seen histologically, the amount of CD31 expression in homogenized tissues increased in a dose-dependent fashion on day 10 post-burn (Fig. 6C). This dose-dependent increase in CD31 is also seen on day 14, with pASC-treated wounds showing slightly lower expression than FPEG alone on day 21 post-burn. By day 42 post-burn, all groups showed a statistically similar amount of CD31 expression. Furthermore, the amount of CD31 expression in homogenized samples (i.e., containing graft and granulation tissue) significantly correlated with the average blood vessel cross sectional area ($p = .0042$) and the percentage of biopsy area represented by blood vessels ($p = .0093$) measured in histological samples from the same wound bed (Fig. 6D).

Supporting Information Figure 2 shows immunohistochemical staining, and Western blotting for VEGF. Representative images of two areas of interest at day 10 are shown for each group, which reveal that a small amount of VEGF expression exists in the superficial areas of tissue (i.e., the epithelium). However, any effect of pASCs on VEGF expression in this area is overcome by the great amount of expression at the junction of the mSTSG in all groups. When quantified, no differences were seen between groups, however there was a biphasic effect of time, wherein VEGF levels were much lower on day 14, higher at day 21, and lower again at day 42. This effect is also evidenced in the representative immunohistochemical images.

pASCs Dose-Dependently Effect Collagen Deposition

To determine the effect of pASCs on collagen deposition in wound remodeling, day 42 samples were analyzed. Representative examples of pictures taken under polarized light after picosirius red staining are shown in Figure 7A. Wound beds treated with

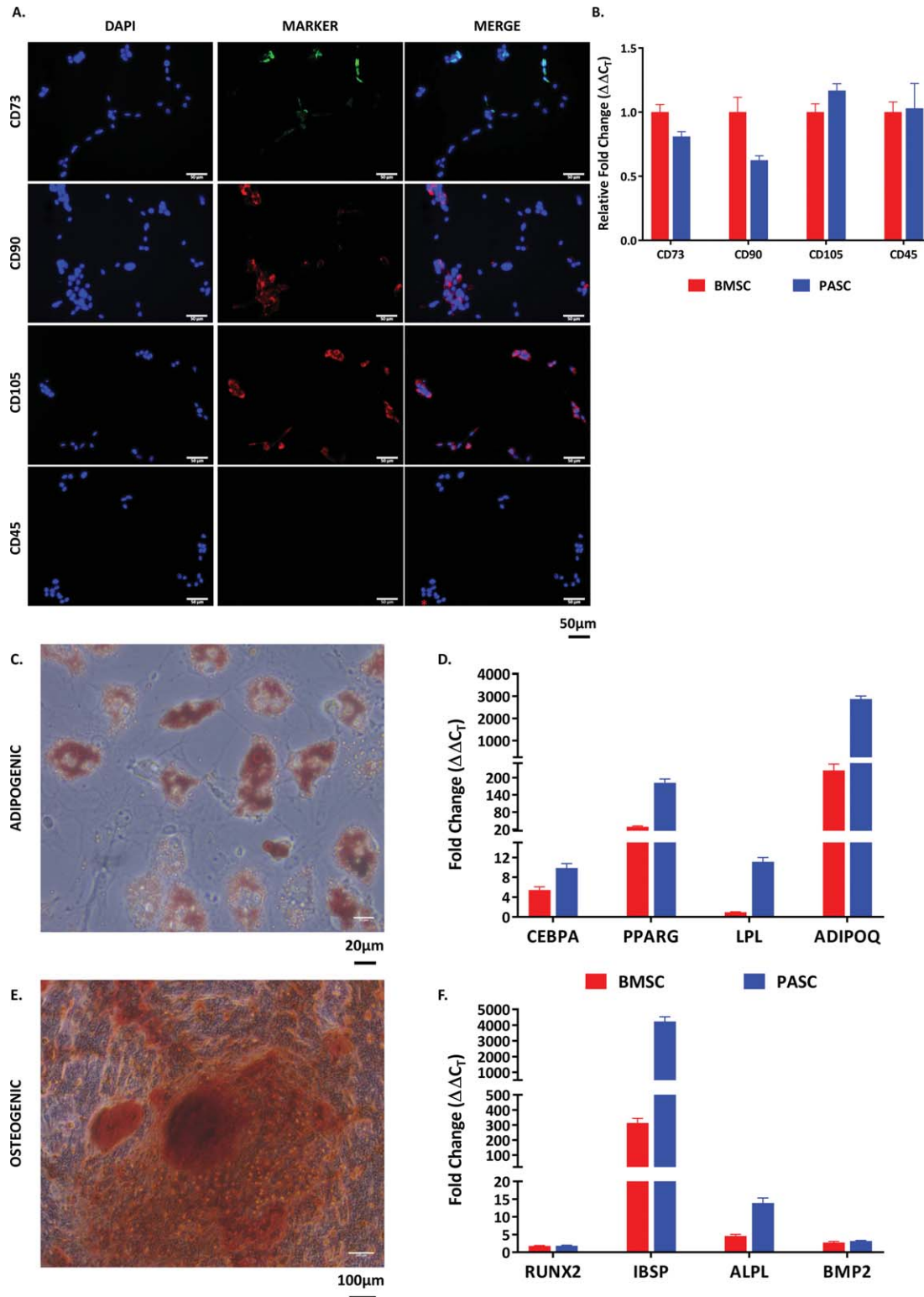


Figure 3. In vitro isolation and characterization of porcine ASCs. **(A):** Isolated pASCs stained positive for antibodies specific for stem cell markers (CD73, CD90, and CD105), while not expressing the leukocyte antigen marker CD45 (scale bar = 50 μ m). **(B):** RT-PCR analysis of these same markers show similar expression of these markers when compared with porcine bone marrow derived stem cells. **(C):** Staining for Oil Red O reveals the adipogenic potential of ASCs (scale bar = 20 μ m), which expressed adipogenic markers **(D)** CEBPA, PPARG, LPL, and ADIPOQ at much higher levels compared with undifferentiated controls. **(E):** Staining for alizarin red reveals osteogenic potential of ASCs (scale bar = 100 μ m), which expressed osteogenic markers **(F)** RUNX2, IBSP, ALPL, and BMP2 at much higher levels compared with undifferentiated controls. Abbreviations: ADIPOQ, adiponectin; ALPL, alkaline phosphatase; BMP2, bone morphogenic protein-2; BMSCs, bone marrow stem cells; CEBPA, CCAAT/enhancer binding protein- α ; IBSP, integrin-binding sialoprotein; LPL, lipoprotein lipase; pASC, porcine adipose-derived stem cell; PPARG, peroxisome proliferator activated receptor- γ ; RUNX2, runt related transcription factor 2.

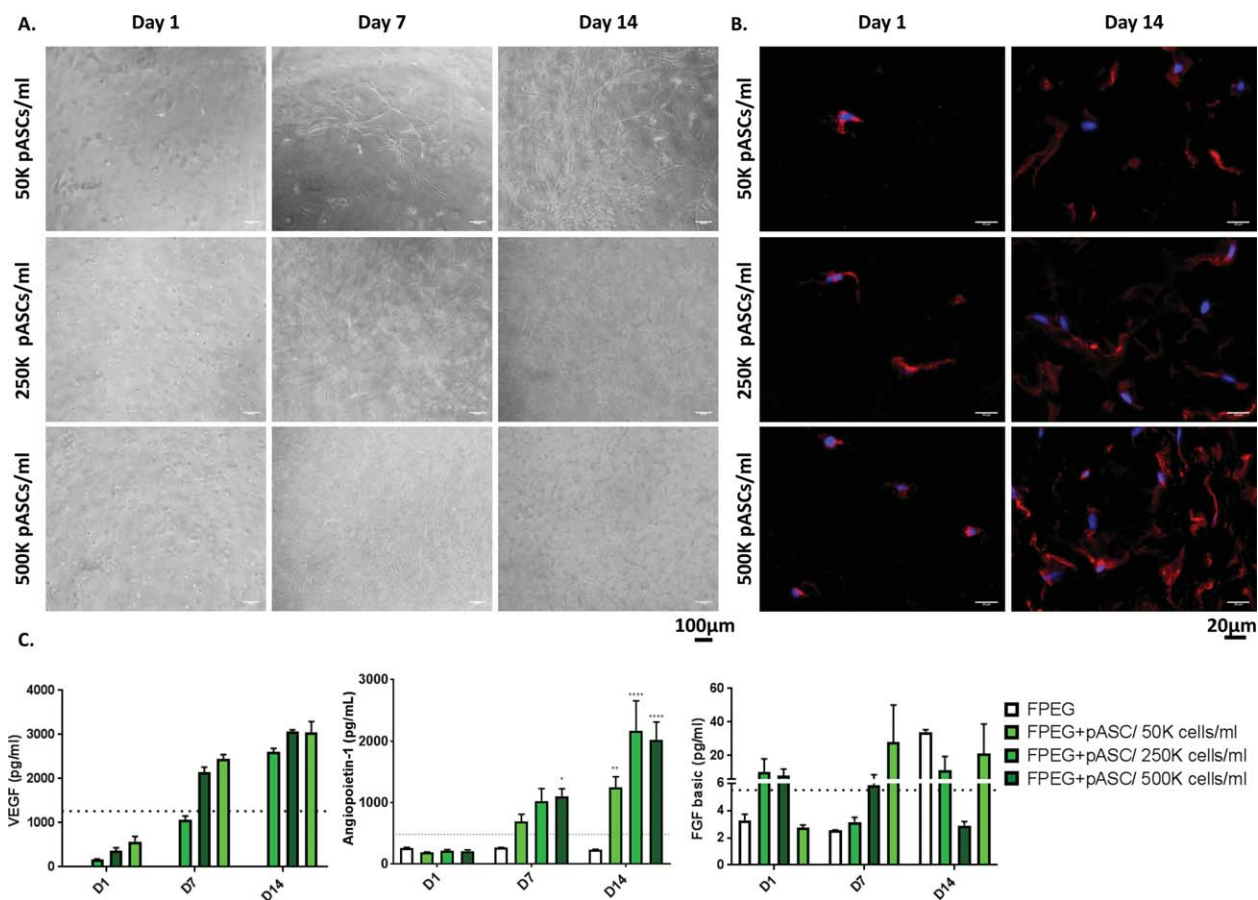


Figure 4. Expansion of porcine ASCs in FPEG hydrogels. **(A):** Light micrographs of ASCs in FPEG hydrogels reveal expansion and connection of ASCs across time (scale bars = 100 μ m). **(B):** Wheat Germ staining also illustrates the dose-dependent increase in ASCs 1 and 14 days after seeding (scale bars = 20 μ m). **(C)** VEGF-A release into the supernatant over time indicates angiogenic growth factor release by ASCs within FPEG hydrogels. Release of Ang-1 followed a similar time course, with significant release shown by days 7, and 14 respectively, while no differences were seen in b-FGF levels. *, $p < .05$; **, $p < .01$; ***, $p < .001$; ****, $p < .0001$ (compared with FPEG). Dotted line represents values from a control monolayer of pASCs. (Scale bars are 100 and 20 μ m). Abbreviations: b-FGF, basic fibroblast growth factor; FPEG, PEGylated fibrin; pASC, porcine adipose-derived stem cell; VEGF, vascular endothelial growth factor.

mSTSG + FPEG alone showed areas of well-organized and dense collagen fibers (bright yellow bands) just deep to the epithelium. Treatment with the lowest concentration of cells (i.e., 50K pASCs/ml) seemed to reduce the prevalence of denser collagen fibers, and led to a more diffuse pattern of collagen (darker/green staining). Upon quantification of the different channels, each wound bed showed drastically lower mean intensity values than the surrounding control tissue, which produced arbitrary unit values of 68.26 ± 2.27 , 24.69 ± 1.10 , and 19.27 ± 0.51 in the red, green, and blue channels, respectively. When comparing treatments, the 500K pASCs/ml group was closest to control values in every color channel, however was only significantly higher in the red channel when compared with FPEG alone (Fig. 7B). Figure 7C shows quantification of total collagen, with a drastically reduced concentration of hydroxyproline in wound beds treated with the lowest amount of cells, which recovers when increasing amounts of pASCs were delivered.

DISCUSSION

The primary findings of the current study is that the combination of FPEG with pASCs represents a feasible adjunct to mSTSG with

the aim of mitigating contraction and accelerating angiogenesis. We were able to successfully isolate pASCs and demonstrate that these cells form networks in vitro when suspended in FPEG hydrogels. We then evaluated the effect of this adjunct therapy in a clinically relevant large animal model. The treatment strategy (i.e., excision and grafting) and wound care (i.e., Xeroform bolsters, dressing changes) used in this study closely follows care of the burned patient. Using this model, we demonstrate both the feasibility and efficacy of applying this therapy in situ to augment meshed STSG after burn wound excision. Together with the allogeneic nature of the pASCs, the translational nature of the current report sets it apart from previous studies looking at FPEG/ASCs in rodent and/or excisional models.

Pig models are considered the best animal models for human skin wound healing for a variety of reasons [33, 34, 47]; however, not many grafting models exist. With the aim of evaluating acute burn wounds, the model used in the current study was based off of a similar model published by Branski et al. with slight modifications [48]. As the previous authors pointed out, following conscious swine for weeks presents certain challenges (e.g., keeping wounds covered) but is addressed with clinical care. It has been noted in similar models that burn wounds can progress past 4

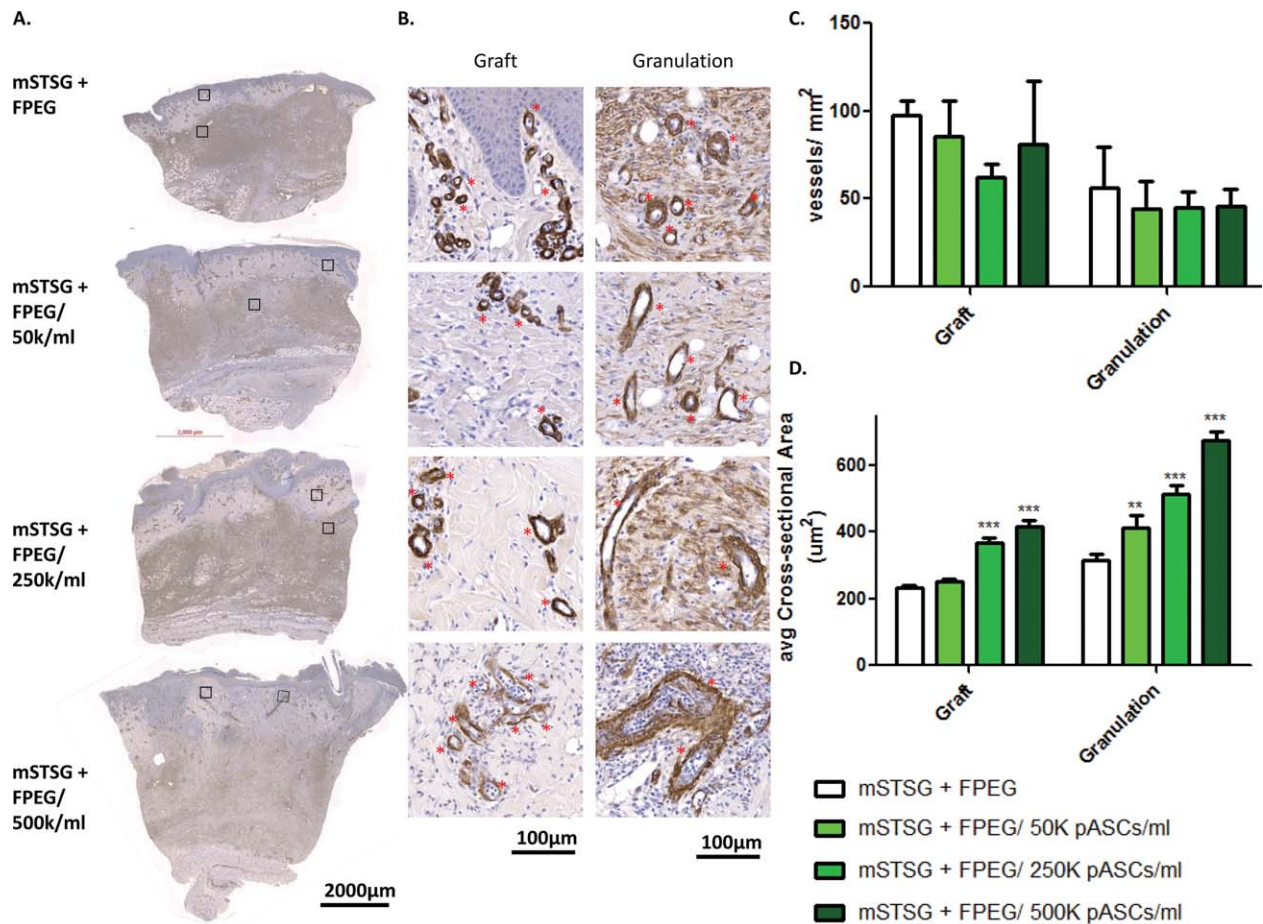


Figure 5. Quantitative comparison of blood vessels within both graft and granulation tissue. **(A):** Representative pictures of biopsies from day 10 post-burn stained with alpha smooth muscle actin (α -SMA) from wounds treated with mSTSG and increasing amounts of pASCs. **(B):** High magnification images of both retained autograft and granulation tissue reveals differences in blood vessels (asterisks), as well as qualitative differences seen in the myofibroblasts (diffuse staining). Quantification of both the average number of blood vessels per mm² **(C)**, and average size of blood vessels **(D)** present within graft and granulation tissue is shown. Two-way ANOVA reveals a dose-dependent effect of pASCs on the size of blood vessels- **, $p < .01$; ***, $p < .001$ (compared with FPEG alone). (Scale bars are 2,000 and 100 μ m). Abbreviations: FPEG, PEGylated fibrin; mSTSG; meshed split thickness skin grafts.

days post-burn [49, 50]; therefore, we decided to debride on day 4 post-burn to allow for progression. While this delay in excision/grafting could theoretically negatively impact graft take, this was not our experience. Previous porcine grafting models have illustrated the beneficial effects of fibrin on graft take [51, 52]. Despite the chemical modification (i.e., PEGylation) used, it is possible that the FPEG treatment does benefit graft adherence. However, the typical clinical practice of Xeroform bolsters and the lack of infection led to good contact between the graft and wound bed, and thus negligible graft failure (i.e., only several instances at the edges due to suture interference).

Other key variables in the current study could potentially underestimate the effect size that FPEG and pASCs had on wound healing parameters (i.e., contraction, reepithelialization). The burn wounds described in this study were made with 3 cm diameter probes, which result in wounds that are roughly 7 cm². Other studies have used wounds up to 50 cm², and larger wounds likely would have contracted more, thus increasing the potential therapeutic window [43, 51, 53]. Additionally, the current study used the minimum meshing ratio of 1:1.5, whereas previous studies have meshed STSG at 1:3. While the 1:1.5 is most often used

clinically, it has been shown that these ratios are consistently overestimated [54]. Despite using a low meshing ratio on a noncritically-sized defect, we were still able to detect increased contraction when STSG were meshed, which was ameliorated when FPEG was applied. Another consequence of the low meshing ratio was that epithelialization emanating from the graft was largely complete in the interstices by day 10 post-burn, although we did see that epithelial thickness was lower with the highest dose of pASCs (Supporting Information Fig. 1). Further studies examining this therapy with different meshing ratios or techniques [55] are certainly warranted.

The beneficial effects of ASCs on wound healing are often attributed to their pro-angiogenic properties. The current study does show that acceleration of angiogenesis (CD31 expression) is achieved with ASC delivery in a dose-dependent fashion. This phenomenon was seen despite potential angiogenic properties of the FPEG itself [56]. Moreover, CD31 expression significantly correlated not with the total number of blood vessels, but rather with the size of blood vessels measured in histopathological biopsies from the same wound. To our knowledge, this is the first evidence showing that ASCs

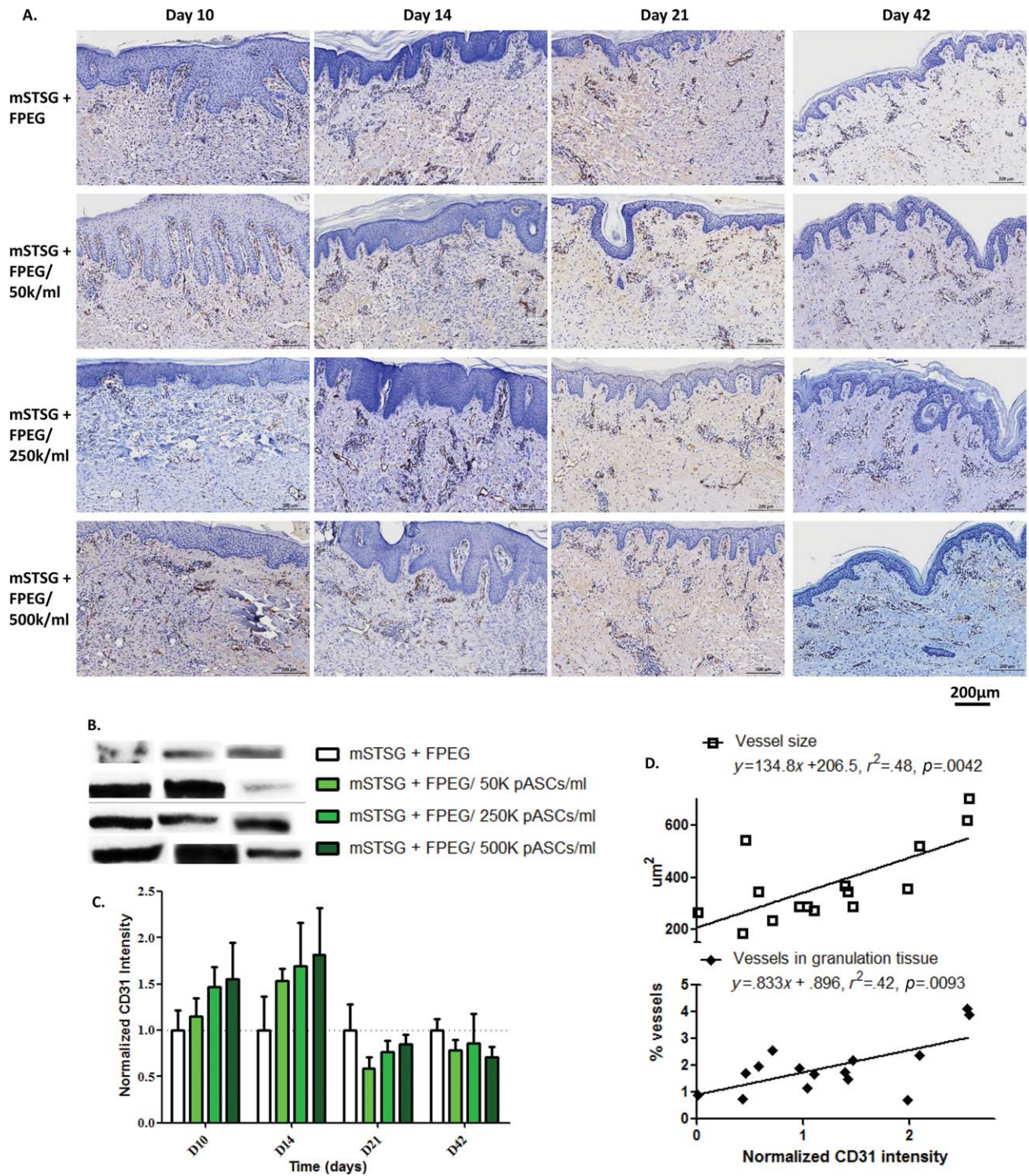


Figure 6. CD31 expression relates to blood vessel size. **(A):** Representative immunohistochemistry for CD31 in each group across time. (Scale bars are 200 µm) **(B)** Representative Western Blot bands for CD31 expression is shown for 3 separate wounds in each group. **(C):** CD31 expression over time shows that pASC delivery accelerates angiogenesis in a dose-dependent fashion, which becomes lower than wounds treated with only mSTSG by day 21 post-burn. By day 42 post-burn, no differences are seen amongst the groups. **(D):** Linear regression analysis of blood vessel size found via histology, and the CD31 expression from the same wounds shows a significant relationship between CD31 expression and both blood vessel cross-sectional area ($p = .0042$) and the percentage of biopsy area taken up by blood vessels ($p = .0093$). Abbreviations: FPEG, PEGylated fibrin; mSTSG; meshed split thickness skin grafts.

may have an enhancing effect on blood vessel size after burn grafting. Vasodilation has been hypothesized to be a potential mechanism of the increase in blood flow due to ASCs [57], and clearly may be a factor in the current model. ASCs have also

been shown to have other effects on wound healing such as acceleration of reepithelialization both in ocular wounds [58] and in cutaneous wounds in diabetic rats [59]. It has also been shown that in a porcine radiation burn model, ASCs accelerate

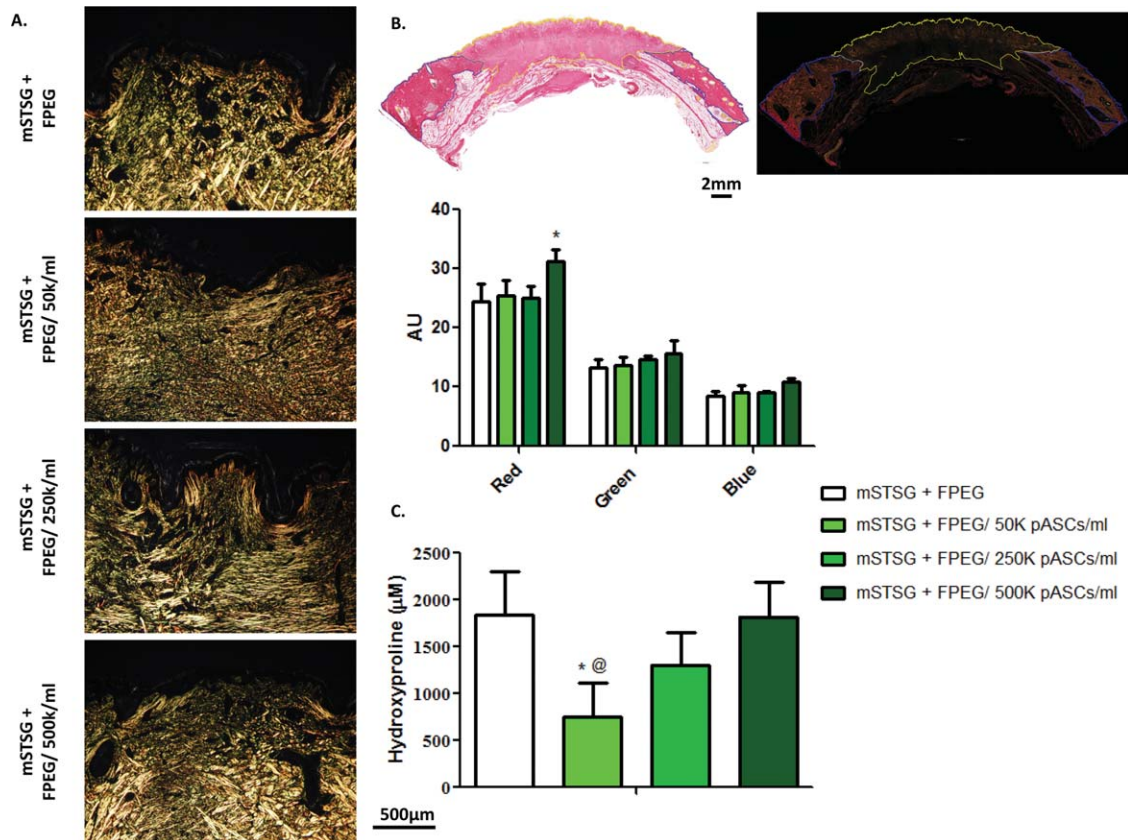


Figure 7. The effect of pASCs on collagen deposition. **(A):** Representative pictures of biopsies stained with picrosirius red and taken under polarized light. An apparent decrease in organized collagen bundles is seen when a low amount of pASCs (50K cells per ml) are added to wounds, which recovers in a dose-dependent fashion. **(B):** Example tracings of the entire day 42 biopsy under brightfield and polarized light which was used to quantify the mean intensity in red, green, and blue channels. Two-way ANOVA reveals that 500K pASCs/ml led to more red intensity than without cells, measured in AU. **(C):** Quantification of total collagen in wound beds from day 42 post-burn shows an initial decrease, and then recovery of collagen content with increasing amounts of cells. (Scale bars are 500 μ m and 2 mm). Abbreviations: AU, arbitrary units; FPEG, PEGylated fibrin; mSTSG; meshed split thickness skin grafts; pASC, porcine adipose-derived stem cell.

angiogenesis and reepithelialization [26]. It is of note that the total number of cells used in this study is orders of magnitude lower than the 200×10^6 ASCs each animal received in the study by Forcheron et al. Moreover, in that study cells were intradermally injected different four times over a 3-month period, while our study used a single application.

The specific mechanisms for the effect of ASCs on collagen deposition in the current study are unclear. It has been shown previously in multiple models that delivery of ASCs reduces collagen deposition and scarring [60, 61]. While we saw lower amounts of collagen after treatment with the lowest dose of ASCs, the amount of collagen increased with increasing amounts of ASCs. Quantification of the PSR stain, however, revealed that the highest dose of ASCs led to more red (thicker) collagen bundles, with no differences in the rest of the groups. Differences in inflammation (which can cause fibrosis) could be a confounding factor [62]. As both ASCs and FPEG have been shown to have immunomodulatory properties, this potential synergism remains to be studied. A caveat of the current report of collagen deposition is the examination at day 42 only. It has been shown in a model of gastrotomy closure, that ASC delivery accelerates collagen deposition acutely (7 days), but reduces collagen deposition by 28 days post-burn [63]. In skin,

where dense collagen bundles are in great abundance, sufficient but not excessive collagen deposition is needed to avoid scarring. The temporal aspects of the mechanisms of collagen deposition also warrant further investigation.

Injectable hydrogels capable of delivering ASCs or other stem cell populations could have enormous impact on wound dressings in not only burns, but also for more general use in plastic surgery. In situ hydrogels are easy to apply and have the advantage of conforming to irregularly shaped wounds. Moreover, while a strategy not used in the current study, the ability to “spray” cells within hydrogels could be combined with different Fibrin and thrombin concentrations to allow for a fine-tuning of gelation time. A variety of different methods exist for initializing hydrogel formation (e.g., photo-crosslinking, enzyme-mediated) which have been reviewed elsewhere [64]. Incorporation of ASCs within chitosan-based hydrogels has demonstrated enhanced angiogenesis in an implantation model [65]. We have recently demonstrated that autologous plasma may be used as a source of fibrinogen to generate hydrogels [38]. While the ASCs used in this study were allogeneic, point-of-care technologies (E.G., Magellan) allow the rapid isolation of ASCs, including from tissue excised from burn patients [25]. Thus, a completely autologous strategy where cells isolated at

the bedside are combined with autologous plasma hydrogels may lead to ultimate biocompatibility.

Several limitations to the current study are worth mentioning. As discussed above, these burn wounds are not critically sized defects and are small enough to likely heal spontaneously. Additionally, the total body surface area affected in these animals was roughly 1%, and the complex pathophysiology/pain that occurs during instances of extensive burns with large TBSA was not recapitulated. Specifically, systemic inflammation and hypermetabolism may alter the specific effect of treatments, including ASCs. Finally, this model was not sufficiently long to investigate any scarring that may have materialized, although the Red Duroc pig is better suited for studying long-term scarring.

CONCLUSION

We have demonstrated that pASCs can be expanded in vitro, combined with FPEG hydrogels at increasing concentrations, and applied in situ. We used a porcine deep partial thickness burn model with excision and grafting to show that this combination represents an attractive adjunct therapy to meshed autografts. By examining FPEG with and without increasing amounts of pASCs, we were able to conclude that, when delivered with meshed autografts, FPEG hydrogels mitigate contraction, while pASCs enhance angiogenesis in vivo. These findings are clinically significant in terms of presenting a feasible and effective therapy that

has the potential to minimize donor sites, accelerate healing, and improve outcomes.

ACKNOWLEDGMENTS

We like to thank the USAISR Veterinary Support Branch and Laboratory Support for their technical assistance. This study was supported by Medical Research and Materiel Command (MRMC). The opinions or assertions contained herein are the private views of the author and are not to be construed as official or as reflecting the views of the Department of the Army or the Department of Defense.

AUTHOR CONTRIBUTIONS

D.B. and S.N.: conception and design, collection and/or assembly of data, data analysis and interpretation, manuscript writing, final approval of manuscript; R.S.: data analysis and interpretation, manuscript writing, final approval of manuscript; N.W., A.L., and S.B.: collection and/or assembly of data, data analysis and interpretation, final approval of manuscript; R.C.: conception and design, financial support, data analysis and interpretation, manuscript writing, final approval of manuscript.

DISCLOSURE OF POTENTIAL CONFLICTS OF INTEREST

The authors indicated no potential conflicts of interest.

REFERENCES

- 1 Peck MD. Epidemiology of burns throughout the world. Part I: Distribution and risk factors. *Burns* 2011;37:1087–1100.
- 2 Janzekovic Z. A new concept in the early excision and immediate grafting of burns. *J Trauma* 1970;10:1103–1108.
- 3 Saaiq M, Zaib S, Ahmad S. Early excision and grafting versus delayed excision and grafting of deep thermal burns up to 40% total body surface area: A comparison of outcome. *Ann Burns Fire Disasters* 2012;25:143–147.
- 4 Akan M, Yildirim S, Misirlioglu A et al. An alternative method to minimize pain in the split-thickness skin graft donor site. *Plast Reconstr Surg* 2003;111:2243–2249.
- 5 Hernandez JL, Savetamal A, Crombie RE et al. Use of continuous local anesthetic infusion in the management of postoperative split-thickness skin graft donor site pain. *J Burn Care Res* 2013;34:e257–e262.
- 6 Robenpour M, Teman J, Tamir G et al. Successful treatment of a 95 per cent body surface area burn. *Burns* 1990;16:462–466.
- 7 Vandeput J, Nelissen M, Tanner JC et al. A review of skin meshers. *Burns* 1995;21:364–370.
- 8 Koljonen V, Gerdin B, Vuola J et al. Non-expandable mesh grafts combine the advantages of mesh grafts and sheet grafts. *Dermatol Surg* 2007;33:831–834.
- 9 Rowan MP, Cancio LC, Elster EA et al. Burn wound healing and treatment: Review and advancements. *Crit Care* 2015;19:243.
- 10 Petry JJ, Wortham KA. Contraction and growth of wounds covered by meshed and non-meshed split thickness skin grafts. *Br J Plast Surg* 1986;39:478–482.
- 11 Schwanholt C, Greenhalgh DG, Warden GD. A comparison of full-thickness versus split-thickness autografts for the coverage of deep palm burns in the very young pediatric patient. *J Burn Care Rehabil* 1993;14:29–33.
- 12 Bello YM, Falabella AF, Eaglstein WH. Tissue-engineered skin. Current status in wound healing. *Am J Clin Dermatol* 2001;2:305–313.
- 13 Bottcher-Haberzeth S, Biedermann T, Reichmann E. Tissue engineering of skin. *Burns* 2010;36:450–460.
- 14 Jeschke MG, Finnerty CC, Shahrokhi S et al. Wound coverage technologies in burn care: Novel techniques. *J Burn Care Res* 2013;34:612–620.
- 15 Supp DM, Boyce ST. Engineered skin substitutes: Practices and potentials. *Clin Dermatol* 2005;23:403–412.
- 16 Brusselaers N, Pirayesh A, Hoeksema H et al. Skin replacement in burn wounds. *J Trauma* 2010;68:490–501.
- 17 Rouwkema J, Rivron NC, van Blitterswijk CA. Vascularization in tissue engineering. *Trends Biotechnol* 2008;26:434–441.
- 18 Butler KL, Goverman J, Ma H et al. Stem cells and burns: Review and therapeutic implications. *J Burn Care Res* 2010;31:874–881.
- 19 Branski LK, Gauglitz GG, Herndon DN et al. A review of gene and stem cell therapy in cutaneous wound healing. *Burns* 2009;35:171–180.
- 20 Cui L, Yin S, Liu W et al. Expanded adipose-derived stem cells suppress mixed lymphocyte reaction by secretion of prostaglandin E2. *Tissue Eng* 2007;13:1185–1195.
- 21 McIntosh K, Zvonic S, Garrett S et al. The immunogenicity of human adipose-derived cells: Temporal changes in vitro. *STEM CELLS* 2006;24:1246–1253.
- 22 Puissant B, Barreau C, Bourin P et al. Immunomodulatory effect of human adipose tissue-derived adult stem cells: Comparison with bone marrow mesenchymal stem cells. *Br J Haematol* 2005;129:118–129.
- 23 Suga H, Glotzbach JP, Sorkin M et al. Paracrine mechanism of angiogenesis in adipose-derived stem cell transplantation. *Ann Plast Surg* 2014;72:234–241.
- 24 Aust L, Devlin B, Foster SJ et al. Yield of human adipose-derived adult stem cells from liposuction aspirates. *Cytotherapy* 2004;6:7–14.
- 25 Natesan S, Wrice NL, Baer DG et al. Debrided skin as a source of autologous stem cells for wound repair. *STEM CELLS* 2011;29:1219–1230.
- 26 Forcheron F, Agay D, Scherthan H et al. Autologous adipocyte derived stem cells favour healing in a minipig model of cutaneous radiation syndrome. *PLoS One* 2012;7:e31694.
- 27 Karimi H, Soudmand A, Orouji Z et al. Burn wound healing with injection of adipose-derived stem cells: A mouse model study. *Ann Burns Fire Disasters* 2014;27:44–49.
- 28 Natesan S, Zamora DO, Wrice NL et al. Bilayer hydrogel with autologous stem cells derived from debrided human burn skin for improved skin regeneration. *J Burn Care Res* 2013;34:18–30.
- 29 Zamora DO, Natesan S, Becerra S et al. Enhanced wound vascularization using a dsASCs seeded FPEG scaffold. *Angiogenesis* 2013;16:745–757.
- 30 Liu H, Collins SF, Suggs LJ. Three-dimensional culture for expansion and differentiation

of mouse embryonic stem cells. *Biomaterials* 2006;27:6004–6014.

31 Zhang G, Wang X, Wang Z et al. A PEGylated fibrin patch for mesenchymal stem cell delivery. *Tissue Eng* 2006;12:9–19.

32 Seetharaman S, Natesan S, Stowers RS et al. A PEGylated fibrin-based wound dressing with antimicrobial and angiogenic activity. *Acta Biomater* 2011;7:2787–2796.

33 Singer AJ, McClain SA. A porcine burn model. *Methods Mol Med* 2003;78:107–119.

34 Sullivan TP, Eaglstein WH, Davis SC et al. The pig as a model for human wound healing. *Wound Repair Regen* 2001;9:66–76.

35 Zuk PA, Zhu M, Mizuno H et al. Multipotent cells from human adipose tissue: Implications for cell-based therapies. *Tissue Eng* 2001;7:211–228.

36 McDaniel JS, Antebi B, Pilia M et al. Quantitative assessment of optimal bone marrow site for the isolation of porcine mesenchymal stem cells. *Stem Cells Int* 2017;2017:1836960.

37 Barthel LK, Raymond PA. Improved method for obtaining 3-microns cryosections for immunocytochemistry. *J Histochem Cytochem* 1990;38:1383–1388.

38 Burmeister DM, Roy DC, Becerra SC et al. In situ delivery of fibrin-based hydrogels prevents contraction and reduces inflammation. *J Burn Care Res* 2017. doi:10.1097/BCR.0000000000000576.

39 Gaines C, Poranki D, Du W et al. Development of a porcine deep partial thickness burn model. *Burns* 2013;39:311–319.

40 Burmeister DM, Cerna C, Becerra SC et al. Noninvasive techniques for the determination of burn severity in real time. *J Burn Care Res* 2017;38:e180–e191.

41 Burmeister DM, Ponticorvo A, Yang B et al. Utility of spatial frequency domain imaging (SFDI) and laser speckle imaging (LSI) to non-invasively diagnose burn depth in a porcine model. *Burns* 2015;41:1242–1252.

42 Ponticorvo A, Burmeister DM, Yang B et al. Quantitative assessment of graded burn wounds in a porcine model using spatial frequency domain imaging (SFDI) and laser

speckle imaging (LSI). *Biomed Opt Express* 2014;5:3467–3481.

43 Wang XQ, Liu PY, Kempf M et al. Burn healing is dependent on burn site: A quantitative analysis from a porcine burn model. *Burns* 2009;35:264–269.

44 Aldridge GM, Podrebarac DM, Greenough WT et al. The use of total protein stains as loading controls: An alternative to high-abundance single-protein controls in semi-quantitative immunoblotting. *J Neurosci Methods* 2008;172:250–254.

45 Taylor SC, Berkelman T, Yadav G et al. A defined methodology for reliable quantification of Western blot data. *Mol Biotechnol* 2013;55:217–226.

46 Taylor SC, Posch A. The design of a quantitative western blot experiment. *Biomed Res Int* 2014;2014:361590.

47 Abdullahi A, Amini-Nik S, Jeschke MG. Animal models in burn research. *Cell Mol Life Sci* 2014;71:3241–3255.

48 Branski LK, Mittermayr R, Herndon DN et al. A porcine model of full-thickness burn, excision and skin autografting. *Burns* 2008;34:1119–1127.

49 Nanney LB, Wenczak BA, Lynch JB. Progressive burn injury documented with vimentin immunostaining. *J Burn Care Rehabil* 1996;17:191–198.

50 Macri LK, Singer AJ, Taira BR et al. Immediate burn excision fails to reduce injury progression. *J Burn Care Res* 2013;34:e153–e160.

51 Branski LK, Mittermayr R, Herndon DN et al. Fibrin sealant improves graft adherence in a porcine full-thickness burn wound model. *Burns* 2011;37:1360–1366.

52 Mittermayr R, Wassermann E, Thurnher M et al. Skin graft fixation by slow clotting fibrin sealant applied as a thin layer. *Burns* 2006;32:305–311.

53 Wang XQ, Kravchuk O, Winterford C et al. The correlation of in vivo burn scar contraction with the level of alpha-smooth muscle actin expression. *Burns* 2011;37:1367–1377.

54 Lyons JL, Kagan RJ. The true meshing ratio of skin graft meshers. *J Burn Care Res* 2014;35:257–260.

55 Henderson J, Arya R, Gillespie P. Skin graft meshing, over-meshing and cross-meshing. *Int J Surg* 2012;10:547–550.

56 Ceccarelli J, Putnam AJ. Sculpting the blank slate: How fibrin's support of vascularization can inspire biomaterial design. *Acta Biomater* 2014;10:1515–1523.

57 Hasdemir M, Agir H, Eren GG et al. Adipose-derived stem cells improve survival of random pattern cutaneous flaps in radiation damaged skin. *J Craniofac Surg* 2015;26:1450–1455.

58 Liu X, Wang Z, Wang R et al. Direct comparison of the potency of human mesenchymal stem cells derived from amnion tissue, bone marrow and adipose tissue at inducing dermal fibroblast responses to cutaneous wounds. *Int J Mol Med* 2013;31:407–415.

59 Loder S, Peterson JR, Agarwal S et al. Wound healing after thermal injury is improved by fat and adipose-derived stem cell isografts. *J Burn Care Res* 2015;36:70–76.

60 Lam MT, Nauta A, Meyer NP et al. Effective delivery of stem cells using an extracellular matrix patch results in increased cell survival and proliferation and reduced scarring in skin wound healing. *Tissue Eng Part A* 2013;19:738–747.

61 Zhang Q, Liu LN, Yong Q et al. Intraleisional injection of adipose-derived stem cells reduces hypertrophic scarring in a rabbit ear model. *Stem Cell Res* 2015;6:145.

62 Eming SA, Martin P, Tomic-Canic M. Wound repair and regeneration: Mechanisms, signaling, and translation. *Sci Transl Med* 2014;6:265sr266.

63 Komiyama S, Sakakura C, Murayama Y et al. Adipose-derived stem cells enhance tissue regeneration of gastrotomy closure. *J Surg Res* 2013;185:945–952.

64 Van Tomme SR, Storm G, Hennink WE. In situ gelling hydrogels for pharmaceutical and biomedical applications. *Int J Pharm* 2008;355:1–18.

65 Cheung HK, Han TT, Marecak DM et al. Composite hydrogel scaffolds incorporating decellularized adipose tissue for soft tissue engineering with adipose-derived stem cells. *Biomaterials* 2014;35:1914–1923.



See www.StemCellsTM.com for supporting information available online.